

# Itinerant ferromagnetism in repulsively interacting spin-orbit coupled Fermi gas

Shang-Shun Zhang<sup>1,2</sup>, Jinwu Ye<sup>2,3</sup>, and Wu-Ming Liu<sup>1</sup>

<sup>1</sup>Beijing National Laboratory for Condensed Matter Physics,

Institute of Physics, Chinese Academy of Sciences, Beijing 100190, China

<sup>2</sup>Department of Physics and Astronomy, Mississippi State University, MS 39762, USA

<sup>3</sup>Key Laboratory of Terahertz Optoelectronics, Ministry of Education,  
Department of Physics, Capital Normal University, Beijing 100048, China

(Dated: October 26, 2019)

We investigate magnetic transitions of repulsively interacting Fermi gases with spin-orbit coupling (SOC). We find that the SOC provides a new and efficient mechanism to realize the itinerant ferromagnetism (FM) which is a long sought state in material science at relatively weak repulsive interactions. The coupling between the density and the spin fluctuations due to the SOC leads to new collective and particle-hole excitations in both paramagnet and FM state, also new quantum to classical crossover regimes near the paramagnet to the FM transition. All these new phenomena are dramatically different from those in conventional Fermi gas without SOC and can be probed by various current experimental techniques.

PACS numbers: 03.75.Ss, 05.10.Cc, 68.35.Rh, 67.80.dk

*Introduction*— Recently the investigation and control of spin-orbit coupling have become subjects of intensive research along at least the following 3 forefronts in condensed matter and cold atom systems: (a) The SOC leads to a new class of insulators called topological insulators [1, 2]. (b) The SOC in correlated electron materials is a critical determining factor leading to a whole new class of electronic states [3] such as various spin-orbital ordered states, spin liquids, various topological phases, etc. (c) Several experimental groups have successfully generated 1D SOC which is a linear combination of Rashba and Dresselhaus SOC, both in Bose and Fermi gas [4–7]. Possible experimental constructions of 2D Rashba or Dresselhaus SOC and 3D Weyl SOC have also been proposed [8, 9]. They inspired extensive theoretical investigations on various important effects of SOC on both spinor Bose-Einstein Condensation and attractive degenerate Fermi gases across BCS to BEC crossover [10]. Topological transitions driven by the SOC on an optical lattice has also been studied [11].

On the other front, realizing the itinerant ferromagnetism (FM) is a long-standing goal in material science dating back to the Stoner’s instability [12]. Nagaoka’s theorem [13], its various extensions [14, 15] and the recent extension to multi-band systems [16] established some rigorous results on itinerant FM in various lattice models. A recent DMRG study of Hubbard ladders [17] points to an itinerant FM in a 2d Hubbard model at some extended fillings and very strong couplings. There have been both experimental [18] and theoretical work [19] on possible FM in a purely repulsively interacting two component Fermi gas of <sup>6</sup>Li atoms. Hertz [20] and Millis [21, 22] constructed a quantum Ginzburg-Landau theory to study magnetic fluctuations near the itinerant paramagnet to itinerant FM transition. But so far, the effects of SOC on the formation of itinerant FM have not been discussed.

In this Letter, we generalize Hertz-Millis theory [20–22] to study magnetic transitions in a repulsively interacting Fermi gas with an isotropic Weyl SOC. We find that the critical interaction strength for the itinerant FM state is greatly reduced due to the flat-band structure near the bottom ( Weyl shell ) of the spectrum ( Fig.1). We develop a path integral formalism where one can extract the system’s collective and Particle-Hole (PH) excitations. In the paramagnet, we find the coupling between density and longitudinal mode leads to one gapless sound mode and one  $L$  mode with a gap  $\Delta_L$  in Fig.2a. There are also two degenerate transverse  $T_1, T_2$  modes with a gap  $\Delta_T = \Delta_L$ . We construct a quantum Ginzburg-Landau effective action with the symmetry breaking pattern  $[SU(2)_{spin} \times SO(3)_{orbit}]_D \rightarrow [U(1)_{spin}^z \times SO(2)_{orbit}]_D$  ( the  $D$  stands for the simultaneous rotation of spin and orbit ) to describe critical magnetic fluctuations near the paramagnet to the FM transition. The coexistence of the  $T_1, T_2$  modes and the  $L$  mode with the different dynamic exponents  $z_T = 3$  and  $z_L = 2$  lead to new quantum-classical crossover regimes in the  $T - \delta_s$  plane ( Fig.2b ). In the FM side, there is a topological Lifshitz phase transition where the 2 Fermi surface (FS) changes into one FS from weak, through intermediate to strong FM ( Fig.3 ). In the weak FM, a small magnetization will make the sound wave velocity anisotropic and also splits one gap into two  $\Delta_L > \Delta_T$ . In the strong FM, only the two  $T_1, T_2$  modes survive the decay into the P-H continuum (Fig.4). We stress dramatic different features between itinerant FM with SOC and those without SOC. In view of the rapid technical developments of cold atoms in speckling, tomographic and *In-Situ* measurements [23–25], our theoretical predictions could be probed in near future experiments in both cold atoms and relevant condensed matter systems.

*General formulation.*—We consider a repulsively interacting two-component Fermi gas with the isotropic Weyl

SOC, described by the Hamiltonian

$$\mathcal{H} = \sum_{\mathbf{k}, \alpha, \beta} \Psi_{\mathbf{k}, \alpha}^\dagger \left( \frac{\hbar^2 \mathbf{k}^2}{2m} + \lambda \mathbf{k} \cdot \boldsymbol{\sigma} - \mu \right)_{\alpha, \beta} \Psi_{\mathbf{k}, \beta} + g \sum_{\mathbf{k}, \mathbf{p}, \mathbf{q}} \Psi_{\mathbf{k}+\mathbf{q}, \uparrow}^\dagger \Psi_{\mathbf{p}-\mathbf{q}, \downarrow}^\dagger \Psi_{\mathbf{p}, \downarrow} \Psi_{\mathbf{k}, \uparrow}, \quad (1)$$

where  $\lambda = \frac{g_F \mu_B \nabla B}{3m\hbar}$  is the SOC strength with  $\nabla B$  the magnetic field gradient in the scheme [8, 9],  $g_F$  the Landé factor and  $\mu_B$  the Bohr magneton,  $g = 4\pi a_s/m$  with  $a_s$  the  $s$ -wave scattering length. The chemical potential  $\mu$  is determined by the density of atoms self-consistently.

The interaction can be divided into the density and spin channel  $\mathcal{H}_I = \frac{g}{2} \int d\mathbf{r} [\rho(\mathbf{r})^2 - \vec{S}(\mathbf{r})^2 + 2\rho(\mathbf{r})]$ , where  $\rho(\mathbf{r}) = \Psi^\dagger \Psi(\mathbf{r})$  and  $\vec{S}(\mathbf{r}) = \Psi^\dagger \vec{\sigma} \Psi(\mathbf{r})$ . In the presence of SOC, the density fluctuation is coupled with the spin fluctuation[26]. We introduce the density-spin order parameter  $\phi_\mu$ ,  $\mu = n, x, y, z$  to decouple the interaction term via a Hubbard-Stratonovich transformation. Integrating out the fermionic fields leads to the effective action for  $\phi_\mu$ :

$$\mathcal{S}_H = \int d\mathbf{r} \int_0^{1/T} d\tau \frac{1}{2g} \phi_\mu^2 - \text{Tr} \ln (-\mathcal{G}_0^{-1} + M), \quad (2)$$

where  $\mathcal{G}_0^{-1} = -\partial_\tau - \mathcal{H}_0 + \mu$ ,  $M = \frac{i}{2} \phi_n \sigma^0 + \frac{1}{2} \vec{\phi} \cdot \vec{\sigma}$ .

In the vicinity of the QCP, the magnetic order parameter  $\vec{\phi}$  can be taken as a small quantity. However, the density channel  $\phi_n$  has a non-zero *imaginary* saddle point value due to the finite particle density of the fermions which could be eliminated by re-defining  $\phi_n$  as the deviation from its saddle point value. To the second order of  $\phi_\mu$ , we obtain  $\mathcal{S}_H^{(2)} = 1/(2\beta V) \sum_{\mathbf{q}, n} \mathcal{K}^{\mu\nu} \phi_\mu(-\mathbf{q}, -i\omega_n) \phi_\nu(\mathbf{q}, i\omega_n)$ , where  $\mathcal{K}^{\mu\nu} = \delta^{\mu\nu}/g - \bar{\chi}^{\mu\nu}(\mathbf{q}, i\omega_n)/4$ ,  $\bar{\chi}^{\mu\nu}$  is related to the usual density and spin susceptibility  $\chi^{\mu\nu}(\mathbf{q}, i\omega_n) = \langle s^\mu(\mathbf{q}, i\omega_n) s^\nu(-\mathbf{q}, -i\omega_n) \rangle$  via  $\bar{\chi}^{00} = -\chi^{00}$ ,  $\bar{\chi}^{0i} = i\chi^{0i}$ ,  $\bar{\chi}^{ij} = \chi^{ij}$  with  $i, j = x, y, z$ .

*Collective modes in the paramagnet phase.*— Adding density-spin sources to Eqn.2, one can extract collective modes through the poles of density and spin correlation functions [26]. In the presence of SOC, it is convenient to define a helical basis with respect to the momentum where we can define two transverse spin modes ( $\hat{T}_1 \cdot \vec{S}$ ,  $\hat{T}_2 \cdot \vec{S}$ ) and one longitudinal spin mode ( $\hat{q} \cdot \vec{S}$ ). In the paramagnet side, the mixing of density and longitudinal mode leads to one gapless sound mode  $\omega_{\mathbf{q}}^s = v_s q$  and one gapped mode  $\omega_{\mathbf{q}}^L = \Delta_s + \beta_L q^2$  called  $L$  mode in Fig.2a. There are also two degenerate gapped transverse modes  $\omega_{\mathbf{q}}^{T_1} = \omega_{\mathbf{q}}^{T_2} = \Delta_s + \beta_T q^2$  just below the  $L$  mode ( Fig.2a ). We find  $\Delta_s$  vanishes for interaction strength larger than  $g_s = 24\pi^2 k_R/m(k_2^2 - k_1^2)$ , where  $k_2 > k_1$  are the two Fermi momenta. This corresponds to an instability in the collective modes channel. In the following section, we will show that the instability in the P-H channel happens

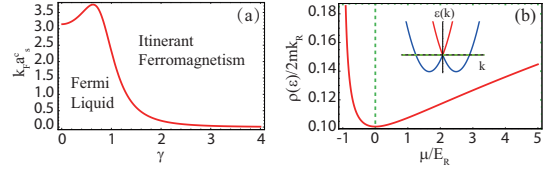


FIG. 1. (Color online) (a): Critical interaction strength  $k_F a_s^c$  as a function of SOC strength  $\gamma = k_R/k_F$ . (b) The Density of states  $\rho(\epsilon)$  in units of  $2mk_R$  at the chemical potential  $\mu$ . The green dashed line denotes  $\mu = 0$  as shown by the inset.

first.

*Ferromagnetic instability.*— There is also a FM instability in the P-H channel when  $\delta = \frac{1}{g_c} - \frac{\chi_0}{4} < 0$ , i.e., the Stoner instability. Here  $\chi_0(\vec{q} \rightarrow 0, \omega/qv_F \rightarrow 0) = \frac{m}{6\pi^2} (\frac{k_1^2 + k_2^2}{K} + \frac{k_2^2 - k_1^2}{k_R})$ ,  $K = \sqrt{k_R^2 + 2m\mu}$ ,  $k_R = m\lambda$  is the static spin susceptibility of 3D free Fermi gas with the Weyl SOC. We obtain the critical value  $k_F a_s^c = F(\gamma)$  as shown in Fig.1 (a), where  $k_F$  is the Fermi momentum without SOC at the same density and  $\gamma = k_R/k_F$ . As  $\gamma$  increases,  $F(\gamma)$  has a maximum at  $\gamma \simeq 0.63$  corresponding to the chemical potential  $\mu = -\frac{2}{3}E_R$  ( $E_R = k_R^2/2m$ ), after which,  $k_F a_s^c$  decreases quickly. At a strong SOC, the  $\mu$  approaches the bottom of the spectrum ( the Weyl shell at  $|\mathbf{k}| = k_R$  ) where the density of states diverges as  $\frac{1}{\sqrt{\epsilon}}$  (see Fig.1 (b)). The effects of an interaction is dramatically enhanced, even a weak interaction will drive the system into the itinerant FM state.

Because  $g_c < g_s$ , so the instability in the P-H channel happens before that in the collective mode channel. So in constructing a quantum Ginzburg-landau action to describe the paramagnet-FM transition, one need to take the  $\mathbf{q} \rightarrow 0, \omega/v_F q \rightarrow 0$  limit to capture the dominant critical spin-fluctuation spectral weights.

*Generalizing the Hertz-Millis effective action to SOC systems.*— Because the density fluctuation is non-critical across the FM phase transition, integrating it out and taking the  $\mathbf{q} \rightarrow 0, \omega/v_F q \rightarrow 0$  limit leads to the effective action in terms of the spin fluctuation order parameter:

$$\mathcal{S}_H = \int \frac{d\mathbf{k}}{(2\pi)^3} T \sum_n \frac{1}{2} \mathcal{G}_s^{-1} \hat{P}_s^{ij} \phi_i \phi_j + u \int d\mathbf{r} d\tau (\vec{\phi}^2)^2, \quad (3)$$

where  $\hat{P}_s^{ij} = \hat{n}_s^i \hat{n}_s^j$  ( $\hat{n}_s = \hat{T}_1, \hat{T}_2, \hat{L}$ ) is the projection operator into the helical basis,  $\mathcal{G}_T^{-1} = \mathcal{G}_{T_1}^{-1} = \delta + \gamma_T y + \alpha_T q^2$  and  $\mathcal{G}_L^{-1} = \delta + \gamma_L y^2 + \alpha_L q^2$  where  $y = |\omega_n|/v_F q$  are the propagators of these helical spin modes. Note that the most relevant interaction term is still  $\mathcal{S}_H^{int} = u \int d\mathbf{r} d\tau (\vec{\phi}^2)^2$  which is  $SU(2)_{spin} \times O(3)_{orbit}$  invariant. There are other quartic terms which contain momenta and only have  $[SU(2)_{spin} \times O(3)_{orbit}]_D$  symmetry, so are less relevant. The effective action takes the same form for  $\mu > 0$  or  $\mu < 0$ . Note that the transverse propagator with the dynamical exponent  $z_T = 3$  is the same

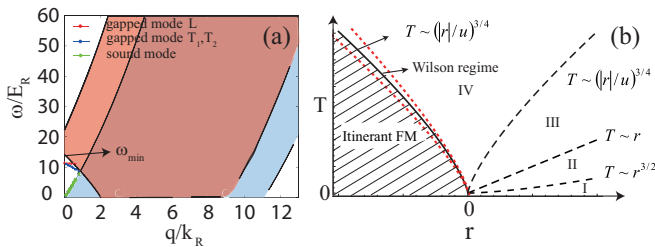


FIG. 2. (Color online) (a) Collective modes and PH excitation in the para-magnet side at  $\gamma = 0.2, a_s = 0.9a_s^c$ . (b) Finite temperature quantum-classical crossovers near the para-magnet to FM transition.  $r$  is the tuning parameter of the transition and  $T$  is the temperature. The boundary between Regime I and II is given by  $T \sim r^{3/2}$  due to the quantum to classical crossover of the two transverse modes, That between Regime II and III is given by  $T \sim r$  due to the quantum to classical crossover of the longitudinal mode. That between Regime III and IV and also the Curie temperature is given by  $T \sim (|r|/u)^{3/4}$  due to the dangerously irrelevant coupling  $u$ . The correlation length  $\xi$  and specific heat coefficient  $\gamma = C_V/T$  display different behaviors in the four regimes and listed in the text [30].

as the FM transition in the ordinary Fermi gas without SOC. While, the longitudinal one with a dynamical exponent  $z_L = 2$  is similar to the Anti-Ferromagnetic (AFM) transition in the ordinary Fermi gas or dilute Bose gas transition without SOC.

*Quantum-Classical crossovers at finite temperatures.*— Under the scaling transformation  $q \rightarrow q'/b, \omega \rightarrow \omega'/b^z, z = 3$ , at the tree level  $\delta' = \delta b^2, \gamma'_L = \gamma_L b^{-2}$  and  $u' = ub^{4-d-z}$ . Because  $4 - (d+z) < 0$  in 3d, so  $u$  is dangerously irrelevant which leads to the violations of scalings holding only below the upper critical dimension[28]. Incorporating the RG flow of the irrelevant  $\gamma_L$  will recover the scaling of the longitudinal mode with the dynamical exponent  $z_L = 2$ . Following the combination of the RG methods developed in [22] and [27], we derived the whole crossover functions in the  $T-r$  plane in Fig.2b for both the correlation length and the free energy. In the following, we only list the qualitative features.

Then, we solve the RG flow equations at one-loop level. Because  $u$  is always irrelevant, we linearize the RG equations in  $u$ . We obtain the renormalized parameters as:  $T(b) = Tb^3, \gamma_L(b) = \gamma_L b^{-2}, u(b) = ub^{-2}$  and

$$\delta(b) = b^2[\delta + 2u \int_0^{\ln b} dx e^{-(1+z_T)x} f_T^{(2)}(Te^{z_T x}) + u \int_0^{\ln b} dx e^{-(1+z_L)x} f_L^{(2)}(Te^{z_L x})]. \quad (4)$$

where, similar to traditional Fermi gas[21],  $f_T^{(2)}(t) \simeq f_T^{(2)}(0) + \mathcal{A}_T t^2$  when  $t \ll 1$ , and  $\simeq \mathcal{B}_T t$  when  $t > 1$ .  $f_L^{(2)}(t)$  behaves similarly except it's temperature depen-

dence is exponentially small for  $t \ll 1$ .

We stop the RG flow at  $\delta(b_*) = 1$  where mean field theory apply. If the renormalized temperature  $Tb_*^{z_T}, Tb_*^{z_L} \ll 1$ , the system stays in the quantum regime as shown by the regime I in Fig. 2. Then  $\delta(b) = b^2(r + u\mathcal{A}_T T^2/r)$  with  $r = \delta - \delta_c$ . The correlation length  $\xi^{-1/\nu} = r + u\mathcal{A}_T T^2/r$  with  $\nu = 1/2$  displays the Fermi liquid behavior. Self-consistency requires  $T \ll r^{z_T \nu} = r^{3/2}$  for this regime I.

In regime II,  $r^{3/2} \ll T \ll r$ , the transverse modes become classical while the longitudinal mode remains quantum-like. The correlation length is given by  $\xi^{-2} = r + 2u\mathcal{C}_T T^{4/3}$  where  $\mathcal{C}_T = \mathcal{A}_T + \mathcal{B}_T$ . The contribution from the longitudinal mode is exponentially small.

In regime III and IV,  $T \gg r$ , both the transverse and the longitudinal mode behaves classically. The correlation length is given by  $\xi^{-2} = r + 2u\mathcal{C}_T T^{4/3} + u\mathcal{C}_L T^{3/2}$  where the contribution from the longitudinal mode is subleading to that from the transverse mode due to  $z_L < z_T$ . Comparing the relative importance of  $r$  and  $2u\mathcal{C}_T T^{4/3}$  leads to  $T \sim (r/2u\mathcal{C}_T)^{3/4}$  separating the two sub-regimes III and IV shown in Fig.2b. Setting  $\xi^{-2} = 0$  leads to the finite Curie temperature  $T_c(r, u) = (-r/2u\mathcal{C}_T)^{3/4}$ . Within a narrow window close to  $T_c(r, u)$ , the system is controlled by the classical Wilson-Fisher fixed point. Note that these two temperatures are set up by the dangerously irrelevant coupling  $u$ .

The free energy density is the sum of that from the two transverse modes  $2F_T$  with  $z_T = 3$  and that from the longitudinal mode with  $z_L = 2$ . The  $F_T$  is the same as that in the traditional Fermi liquid [22]. The  $F_L$  is given by a universal function  $F_L(r, T) = T^{5/2} \Phi_L(\frac{r}{T})$  [29]. In the quantum regime of longitudinal mode I/II,  $T/r \ll 1$ , the specific-heat coefficient  $\gamma = C_V/T = \frac{\mathcal{A}_1}{r^{3/2}} T^2$  where  $\mathcal{A}_1 \simeq 1.316$ . While in classical regime III/IV,  $T/r \gg 1$ ,  $\gamma = \mathcal{A}_2 T^{1/2}$  where  $\mathcal{A}_2 \simeq 0.113$ .

*Properties in the itinerant FM side.*— For  $g > g_c$  ( $\delta_s < 0$ ), it moves to the ferromagnetic side, the magnetization  $\langle \vec{\phi} \rangle = -\frac{g}{2} \langle \vec{M} \rangle \neq 0$  can pick up any direction ( such as  $z$  direction ) which breaks the  $[SU(2)_{spin} \times O(3)_{orbit}]_D$  symmetry in the effective action Eqn.3 to  $[U^z(1)_{spin} \times U^z(1)_{orbit}]_D$ . We find  $M \sim (g - g_c)^{1/2}$  from the self-consistent equation which is the same critical exponent as the traditional case. Then we can re-define  $\phi_{T1}, \phi_{T2}, \phi_L$  with respect to this direction ( Note that they are defined with respect to the momentum  $\vec{q}$  in the para-magnet side ). The fermionic spectrum as shown in Fig. 3 (a)-(c) is given by

$$\xi_{\mathbf{k},s} = k_\perp^2 + k_z^2 + 2s\sqrt{k_\perp^2 + (k_z - \zeta)^2}, \quad (5)$$

where  $s = \pm, k_\perp = \sqrt{k_x^2 + k_y^2}$ . We have taken the momentum unit  $k_R = m\lambda$  and energy unit  $E_R = k_R^2/2m$ . The dimensionless value  $\zeta = \frac{Mg}{4\lambda k_R}$  which denotes the strength of magnetization is the crossing point of the two

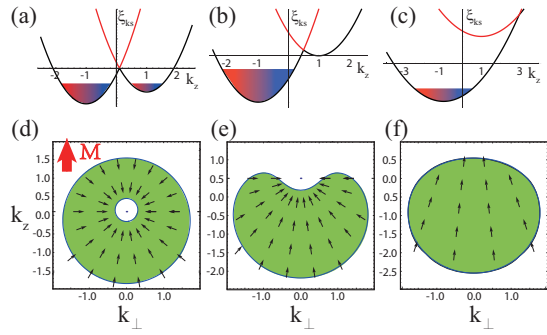


FIG. 3. (Color online) Evolution of fermionic spectrum  $\xi_{\mathbf{k}s}$  (upper panel) and Fermi surfaces (down panel) at the SOC strength  $\gamma = 0.74$  with increasing magnetization strength  $\zeta$  at  $\zeta = 0.1$  for (a),(d),  $\zeta = 0.5$  for (b),(e),  $\zeta = 3$  for (c),(f). The spectrum has a rotational symmetry about  $k_z$  axes. The black arrows show the spin polarization. There is a topological Lifshitz phase transition where the 2 FS changes into one FS near  $\zeta \sim 1$ .

helicity branches. The spectrum in Fig.3 has a global minimum at  $\mathbf{k} = -1\hat{e}_z$ , independent of the value of  $\zeta$ . The magnetization  $\vec{M}$  induces a FS shift along the  $\hat{k} = -\hat{z}$  with the  $[U^z(1)_{spin} \times U^z(1)_{orbit}]_D$  rotation symmetry. However, the local current density vanishes due to the presence of the SOC [31]. The symmetry breaking leads to two gapped transverse pseudo-Goldstone modes. For an given particle density with increasing  $\zeta$ , we divide the FM phase into three regimes shown in the Fig.3.

In the weak FM near to the QCP:  $\zeta \ll 1$  ( Fig.3a,3d), there are still 2 FS. There is still one gapless sound mode and three gapped modes (see Fig.2a). However, due to the symmetry breaking in the FM side, the effects of the small magnetization in Fig.2a are (1) the sound wave velocity becomes anisotropic  $\omega = v(\theta)q$ . (2) One gap in paramagnet side splits into two:  $\Delta_L > \Delta_T$  and the dispersion near  $\mathbf{q} = 0$  is linear along  $q_z$  direction. All the collective modes are still outside the P-H spectrum, therefore remain stable. It is important to stress that this gapless sound mode is not a Goldstone mode. Because the spin-momentum locking, the symmetry breaking  $[SU(2)_{spin} \times O(3)_{orbit}]_D \rightarrow [U^z(1)_{spin} \times U^z(1)_{orbit}]_D$  only leads to gapped pseudo-Goldstone modes instead of gapless Goldstone modes, in sharp contrast to the  $SU(2)_{spin} \rightarrow U^z(1)_{spin}$  symmetry breaking in conventional Fermi systems without SOC.

As  $\vec{M}$  increases, there is a topological Lifshitz phase transition [11] where the 2 FS changes into one FS near  $\zeta \sim 1$  ( Fig.3b,3e). The spin polarization changes as shown by the arrows. Due to the complicated FS geometry in Fig 5e, one can only perform numerical calculations on the two transverse modes and the corresponding intra- and inter-band P-H excitation spectra. We find that the sound ( L ) mode will start to fall into the intra-band ( inter-band ) P-H continuum, therefore over-damped,

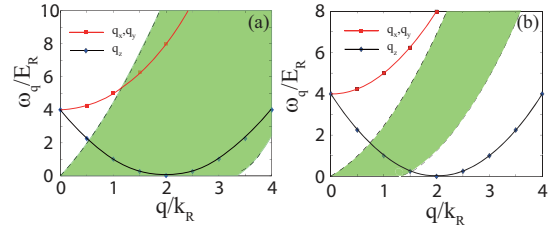


FIG. 4. (Color online) The Intra-band ( - helicity ) P-H excitation spectrum along  $q_z$  direction (green regimes) and collective modes for near saturation case  $\zeta \gg 1$ . (a) plots dense density case and (b) plots dilute density case. Due to its very high energy, inter-band one is not shown.

then only the two transverse pseudo-Goldstone modes survive the Lifshitz phase transition. Then we only need to focus on the behaviors of the two pseudo-Goldstone modes after the Lifshitz phase transition.

In the strong FM:  $\zeta \gg 1$  ( Fig.3c,3f), there is a large energy separation between the two helicities. In the  $\zeta \rightarrow \infty$  limit, the ”-” helicity band approaches a spherical Fermi surface centered at  $\hat{k} = -\hat{z}$ :  $\xi_{\mathbf{k},s} = (\mathbf{k} - s\hat{e}_z)^2 - 2s\zeta - 1, s = \pm 1$ . The spin approaches being polarized along the  $\hat{z}$  axis ( Fig.5f). One can perform analytical calculations in such a simplified FS geometry and obtain the dispersion of the two transverse pseudo-Goldstone modes. They have an energy gap  $\sim 4E_R$  at  $\mathbf{q} = 0$ , behave as  $\omega_{\mathbf{q}} = (\mathbf{q} - 2\hat{e}_z)^2/5$  near the roton minimum at  $\mathbf{q} = 2\hat{e}_z$ . At large, but finite  $\zeta$ , the dispersion obtains a small imaginary part inside the intraband P-H excitation shown in Fig. 4. The roton mode acquires a tiny gap [32].

*Experimental implementation and summary.*— In a  ${}^6\text{Li}$  system, the two hyperfine sublevels  $|1/2, -1/2\rangle$  and  $|1/2, 1/2\rangle$  can be chosen as two spin-1/2 states. With  $N \sim 10^4$   ${}^6\text{Li}$  atoms inside an isotropic trap with a trap frequency  $2\pi \times 10\text{Hz}$ , and a typical magnetic field gradient strength  $\nabla B = 0.09\text{G}/\mu\text{m}$  (within practical range [33]), we estimate the critical interaction strength as  $k_F a_s^c \simeq 0.19$ , which is order of magnitude smaller than the value  $\simeq 3\pi/4$  without the SOC [19, 20]. In the itinerant FM, monitoring spin fluctuations using speckle imaging could provide evidences of formation of magnetic domains [23]. From a high resolution density image of atoms in a trap at finite temperature, one can also extract information about their critical behaviors [24, 25].

In Summary, a strong SOC in repulsively interacting Fermi systems creates a rare favorable condition to realize a new kind of itinerant FM state which is a long sought state in condensed matter systems. The collective and PH excitations in both paramagnet and FM display dramatically different properties than their counterparts without SOC. The two types of critical fluctuations with two different dynamic exponents  $z_T = 3$  and  $z_L = 2$  lead to new finite temperature quantum to classical crossover

regimes. Furthermore, the itinerant FM also displays the anomalous Hall effect [34] and will be investigated in a future publication. These new phenomena can be probed by current experimental techniques in cold atoms and condensed matter systems. This work can be easily generalized to other types of SOC.

This work was supported by the NKBRFC under grants Nos. 2011CB921502, 2012CB821305, NSFC under grants Nos. 61227902, 61378017, 11311120053. J. Ye was supported by NSF-DMR-1161497, NSFC-11074173, 11174210, Beijing Municipal Commission of Education under Grant No. PHR201107121.

- 
- [1] M. Z. Hasan and C. L. Kane, *Rev. Mod. Phys.* **82**, 3045 (2010).
- [2] X. L. Qi and S. C. Zhang, *Rev. Mod. Phys.* **83**, 1057 (2011).
- [3] For example, see " Exotic Phases of Frustrated Magnets " conference held at KITP October 8-12, 2012. <http://online.kitp.ucsb.edu/online/fragnets-c12/>
- [4] Y. J. Lin, K. Jiménez-García, and I. B. Spielman, *Nature (London)* **471**, 83 (2011).
- [5] P. Wang, Z. Q. Yu, Z. Fu, J. Miao, L. Huang, S. Chai, H. Zhai, and J. Zhang, *Phys. Rev. Lett.* **109**, 095301 (2012).
- [6] L. W. Cheuk, A. T. Sommer, Z. Hadzibabic, T. Yefsah, W. S. Bakr, and M. W. Zwierlein, *Phys. Rev. Lett.* **109**, 095302 (2012).
- [7] For a review, see J. Dalibard, F. Gerbier, G. Juzeliūnas, and P. Öhberg, *Rev. Mod. Phys.* **83**, 1523 (2011).
- [8] B. M. Anderson, I. B. Spielman, and G. Juzeliūnas, *Phys. Rev. Lett.* **111**, 125301 (2013).
- [9] Z.-F. Xu, L. You, and M. Ueda, *Phys. Rev. A* **87**, 063634 (2013); Z. -F. Xu and L. You, *Phys. Rev. A* **85**, 043605 (2012).
- [10] C. Wang, C. Gao, C. M. Jian, and H. Zhai, *Phys. Rev. Lett.* **105**, 160403 (2010); T. -L. Ho and S. Zhang, *Phys. Rev. Lett.* **107**, 150403 (2011); Z. Q. Yu and H. Zhai, *Phys. Rev. Lett.* **107**, 195305 (2011); H. Hu, L. Jiang, X. -J. Liu, and H. Pu, *Phys. Rev. Lett.* **107**, 195304 (2011); H. Hu, B. Ramachandran, H. Pu, and X. -J. Liu, *Phys. Rev. Lett.* **108**, 010402 (2012); C. Qu, Z. Zheng, M. Gong, Y. Xu, L. Mao, X. Zou, G. Guo, and C. Zhang, *Nat. Commun.* **4**, 2710 (2013); W. Zhang and W. Yi, *Nat. Commun.* **4**, 2711 (2013). J. P. Vyasankere and V. B. Shenoy, *Phys. Rev. B* **83**, 094515 (2011); J. P. Vyasankere, S. Zhang and V. B. Shenoy, *Phys. Rev. B* **84**, 014512 (2011). Qi Zhou and Xiaoling Cui, *Phys. Rev. Lett.* **110**, 140407.
- [11] Fa-Di Sun, Xiao-Lu Yu, Jinwu Ye, Heng Fan, W. M. Liu, *Scientific Reports* **3**, 2119 (2013).
- [12] E. Stoner, *Philos. Mag.* **15**, 1018 (1993).
- [13] Y. Nagaoka, *Phys. Rev.* **147**, 392 (1966).
- [14] A. Mielke, *J. Phys. A: Math. Gen.* **24**, L73 (1991); **24**, 3311 (1991); *Phys. Lett. A* **174**, 443 (1993).
- [15] H. Tasaki, *Phys. Rev. Lett.* **69**, 1608 (1992); *Phys. Rev. B* **40**, 9192 (1989); *Commun. Math. Phys.* **242**, 445 (2003); A. Tanaka and H. Tasaki, *Phys. Rev. Lett.* **98**, 116402, (2007).
- [16] Y. Li, E. H. Lieb, and C. Wu, arxiv: 1310.4391.
- [17] Li Liu, Hong Yao, Erez Berg, Steven R. White, and Steven A. Kivelson, *Phys. Rev. Lett.* **108**, 126406 (2012).
- [18] G. B. Jo, Y. R. Lee, J. H. Choi, C. A. Christensen, T. H. Kim, J. H. Thywissen, D. E. Pritchard, and W. Ketterle, *Science* **325**, 1521 (2009).
- [19] R. A. Duine and A. H. MacDonald, *Phys. Rev. Lett.* **95**, 230403 (2005); V. B. Shenoy and T.-L. Ho, *Phys. Rev. Lett.* **107**, 210401 (2011); D. Pekker, M. Babadi, R. Sensarma, N. Zinner, L. Pollet, M. W. Zwierlein, and E. Demler, *Phys. Rev. Lett.* **106**, 050402 (2011); S. Pilati, G. Bertainia, S. Giorgini, and M. Troyer, *Phys. Rev. Lett.* **105**, 030405 (2010). X. Cui and T.-L. Ho, *Phys. Rev. Lett.* **110**, 165302 (2013); *Phys. Rev. A* **89**, 023611 (2014).
- [20] J. A. Hertz, *Phys. Rev. B* **14**, 1165 (1976).
- [21] A. J. Millis, *Phys. Rev. B* **48**, 7183 (1993).
- [22] U. Zülicke and A. J. Millis, *Phys. Rev. B* **51**, 8996 (1995).
- [23] C. Sanner, E. J. Su, A. Keshet, W. Huang, J. Gillen, R. Gommers, and W. Ketterle, *Phys. Rev. Lett.* **106**, 010402 (2011); C. Sanner, E. J. Su, W. Huang, A. Keshet, J. Gillen, and W. Ketterle, *Phys. Rev. Lett.* **108**, 240404 (2012).
- [24] Y. Shin, C. H. Schunck, A. Schirotzek, and W. Ketterle, *Nature (London)* **451**, 689 (2008).
- [25] N. Gemelke, X. Zhang, C. -L. Huang, and C. Chin, *Nature (London)* **460**, 995 (2009).
- [26] S. S. Zhang, X. L. Yu, J. Ye, and W. M. Liu, *Phys. Rev. A* **87**, 063623 (2013).
- [27] Jinwu Ye and S. Sachdev; *Phys. Rev. Lett.* **80**, 5409 (1998); Jinwu Ye; *Phys. Rev. B* **58**, 9450 (1998); Jinwu Ye, *Phys. Rev. B* **60**, 8290 (1999).
- [28] A. Chubukov, S. Sachdev and J. Ye ; *Phys. Rev. B* **49**, 11919 (1994).
- [29] The universal function is defined as:  $\Phi_L(x) = \frac{K_3}{2} \int_0^\infty dt t^{-5/2} \ln[1 - \exp(-\frac{1}{t}\sqrt{1+xt})]$ , where  $K_3 = 1/2\pi^2$  is an angle integration factor in 3D. The asymptotic form of  $\Phi_L(x)$  in quantum regime I and II,  $x \gg 1$ , is given by  $\Phi_L(x) \simeq -K_3 C_1 / (2x^{3/2})$ , where  $C_1 \simeq 4.3292$ ; while in classical regime III and IV,  $x \ll 1$ , there is  $\Phi_L(x) \simeq -K_3 C_2 / 2$ , where  $C_2 \simeq 1.18886$ . The irrelevant interaction  $u$  provides small corrections near the critical point.
- [30] Note that the quantum critical theory from the normal to FM ( or AFM ) transition even without SOC is still not completely understood. A more refined GL theory should treat both the order parameter fluctuations and the gapless fermions with the two helicities on the same footing and remain to be constructed. For example, in Fermi systems without SOC, see Thomas Vojta, D. Belitz, R. Narayanan, T.R. Kirkpatrick, *Z. Phys. B* vol. 103, pp. 451-461 (1997). T. Senthil, Matthias Vojta, and Subir Sachdev, *Phys. Rev. B* **69**, 035111 (2004). For a review, see H. V. Lohneysen, A. Rosch, M. Vojta, and P. Wolfle, *Rev. Mod. Phys.* **79**, 1015 (2007).
- [31] The ground state average of the supercurrent is given by:  $\mathbf{j} = \mathbf{j}_k + \mathbf{j}_s$  with  $\mathbf{j}_k = (2/V) \sum_{\mathbf{k},s} \mathbf{k} n_{\mathbf{k},s}$  and  $\mathbf{j}_s = (2/V) \sum_{\mathbf{k},s} \vec{S}_{\mathbf{k},s} n_{\mathbf{k},s}$ , where  $n_{\mathbf{k},s} = \Theta(\mu - \xi_{\mathbf{k},s})$ ,  $\vec{S}_{\mathbf{k},s} = s(k_x, k_y, k_z - \zeta) / \sqrt{k_x^2 + k_y^2 + (k_z - \zeta)^2}$  is the spin vector for state  $|\mathbf{k}, s\rangle$ . It is easy to show that  $\mathbf{j} = 0$  for  $\zeta \rightarrow \infty$  and holds for arbitrary  $\zeta$  and  $\mu$  through numerical calculation.
- [32] It is interesting to compare with the counterpart modes in the conventional itinerant FM. In this conventional

itinerant FM, the two transverse modes with the dispersion  $\omega \sim Dq^2$  are out of the interband P-H continuum, so are stable, while the mixed longitudinal-density modes are inside the intra-band P-H continuum, so are over-damped. The crucial difference here is that the two transverse modes are gapped in the SOC case due to the

locking of spin polarization to the FS shift along  $\vec{k} = -1\hat{z}$ , but they are gapless with the dispersion  $\omega \sim Dq^2$  in the conventional case. This fact leads to main experimental signature of a strong itinerant FM in the SOC system.

- [33] M. Trinker, *et.al*, Appl. Phys. Lett. **92**, 254102 (2008).
- [34] Jinwu Ye, *et al*, Phys. Rev. Lett. 83, 3737 (1999).